

First-principles lattice-gas Hamiltonian revisited: O-Pd(100)

Wolfgang Kappus

wolfgang.kappus@t-online.de

v1: 2016-12-04

Abstract

The methodology of deriving an adatom lattice-gas Hamiltonian (LGH) from first principles (FP) calculations is revisited. Such LGH expansions compute lateral interactions by solving a set of linear equations describing regular adatom configurations and their FP energies. The basic assumption of truncating interaction terms beyond fifth nearest neighbors does not hold when adatoms show longer range interactions, e.g. substrate mediated elastic interactions. O-Pd(100) as a popular reference is used to propose a long range elastic interaction alternative including trio- and quattro terms with just 3 parameters fitted to FP calculations. Adatom pair distributions are derived up to half coverage using an adapted Boltzmann distribution and compared with LEED data. A scaling scheme for varying temperatures is provided. Adatom three-body distributions are used to analyze adatom near order. Long range order of adatoms is not found with the elastic model. The assumptions made are discussed and ways to further verify and apply the model are outlined.

1. Introduction

Interactions of adatoms are a subject of continuous interest, various different interaction mechanisms have been described in detail [1]. Adatom structures like superlattices, nanodot arrays, nanostripes, strain relief patterns are interesting for various general and technological reasons; reviews were given in [2,3,4,5]. Lateral interactions also govern the ordering behavior of adatoms and thus the catalytic activities of surfaces [6]. Lattice models are the discrete representations of surface properties and usable for predicting structure and phase diagrams of adatom configurations [1].

Thanks to computational power and advanced algorithms the lateral interactions of adatoms have been determined from first principles using density-functional theory (DFT) and used as inputs to derive lattice-gas Hamiltonians

(LGHs) [7]. The accuracy of this method was analyzed for the O-Pd(100) system and its results were applied to understand surface ordering of atomic adsorbates at that system [8]. These first principle calculations determined the location of O adatoms preferably on fourfold coordinated surface sites. The subsequent lattice gas expansion postulated trio (triplet) and quattro (quadruplet) interactions to fit the DFT results. Those calculations focused on the range up to about half coverage since experiments showed the onset of surface reconstruction when the coverage is increased beyond half coverage [9].

Key assumption in those calculations were vanishing interactions from 6th next neighbors, allowing to derive short range lateral interaction energies from ordered adatom configurations with systems of linear equations.

Since similar calculations of the O-Ag(111) system showed significant lateral displacements [10] the question is raised in the following, what impact longer range interactions may have also in the O-Pd(100) system. An s^{-3} type interaction would lead to an s^{-1} dependency in lattice sums and show results quite different from short range interactions.

In the following DFT results of [8] for the O-Pd(100) system will be interpreted in terms of elastic adatom interactions and an appropriate lattice gas Hamiltonian will be derived. To facilitate the comparison of the two approaches the terminology of [8] will be used in parts.

Strain mediated adatom interactions with the basic s^{-3} distance proportionality and the strong influence of the substrates elastic anisotropy were discussed already in the 1970 decade based on elastic continuum theory [11,12,13]. Usage of an elastic mode theory [14] allowed to handle the s^{-3} singularity at the origin [12]. A review of elastic effects on surface physics was given in [15].

The results of [8] for the O-Pd(100) system claim the relevance of trio- and quattro interactions; this caused an extension of the pair interaction theory of [12]. The presentation of such extension would overload this analysis and therefore is given elsewhere [16].

In the pair interaction model of [12] the interaction of adatoms is mediated by their strain fields generated by single adatoms exerting isotropic stress to their vicinity. Isotropic stress is a consequence of adatom locations on sites with 4-fold symmetry. In a lattice description adatoms would exert forces to their immediate substrate neighbors creating a displacement field equivalent to a strain field. In other cases where adatoms interact directly e.g. via their dipole moment or via electronic overlap, pairs of adatoms may create substrate strain by stretching or compressing the substrate to balance the forces. The strain field of such pairs will mediate interactions between pairs and also between pairs and monomers, an interpretation of trio and quattro interactions. If forces between dimer constituents are central, the model can be kept simple and the resulting stress field can (with symmetry restrictions) be described with one more free parameter than the previous pair interaction model [16].

Since within [8] DFT-calculated energies for only a few ordered adatom configurations have been published, the comparison between the elastic model and the DFT results must stay incomplete for the time being.

Instead of using a Monte Carlo simulation for evaluating the system partition

function and order parameters like in [8], a pair distribution analysis based on [17, 18] will be performed. Together with the resulting three-body distribution this will allow to derive the adatom neighborhood at various coverages. The temperature dependence of the pair distribution will be given by a simple scaling law.

The Fourier transform of the adatom correlation will allow comparisons with LEED measurements of the O-Pd(100) system [19].

The paper is organized as follows:

After outlining the general motivation in section 1, basic interaction model details are recalled in section 2. In section 3 model parameters are fitted to the first principles calculations of [8]. In section 4 the pair distribution analysis is performed and adatom ordering is discussed. In section 5 applicability and limitations of the model are discussed and open questions are addressed. Section 6 closes with a summary of the results.

2. Adatom Interaction Model

In this section the lattice-gas Hamiltonian is employed in which the total free binding energy of one component configurations are expanded in sums of discrete interactions between lattice sites. These discrete interactions are related to the energy of configurations calculated by first principles methods as done for O-Pd(100) in [8].

2.1. Lattice-gas Hamiltonian

The total free binding energy H is assumed to be a sum of site energies $F_b^{\text{on-site}}$, pair interactions V_{ij} , trio interactions V_{ijk} and higher terms

$$H = F_b^{\text{on-site}} \sum_i n_i + \sum_i \sum_{j < i} V_{ij} n_i n_j + \sum_i \sum_{j < i} \sum_{k < j < i} V_{ijk} n_i n_j n_k + (2.1)$$

with occupation numbers n_i . The discrete interactions will not individually be derived from DFT calculations as in [8] but taken from a substrate strain mediated interaction model outlined in the following section.

2.2. Elastic interaction model

The occurrence of trio- and quatto interactions in [8] causes an extension of current elastic pair interaction models. While elastic pair interactions are related to the stress fields of single adatoms, adatom dimers will generate elastic trio- and quatto interactions in the following model, a condensed version of [16].

Adatoms or dimers exert forces on their substrate neighbors leading to a displacement of substrate atoms to balance those forces. Such displacements will increase or decrease the energy of neighboring adatoms or dimers. In a continuum description adatoms and dimers exert stress parallel to the surface

leading to substrate strain which in turn can lead to an attraction or a repulsion of neighboring adatoms or dimers. It will be shown that the strength of such strain mediated interaction will depend on the stress adatoms or dimers exert on the substrate and on the stiffness of the substrate.

The elastic energy of a substrate with adatoms in a continuous description is given by the sum of two parts, the energy of the distorted substrate and the energy of adatoms exerting tangential forces on the substrate

$$H_{\text{el}} = \frac{1}{2} \int_V \boldsymbol{\epsilon}(\mathbf{r}) \mathbf{c} \boldsymbol{\epsilon}(\mathbf{r}) d\mathbf{r} + \int_S \boldsymbol{\epsilon}(\mathbf{s}) \boldsymbol{\pi}(\mathbf{s}) d\mathbf{s}. \quad (2.2)$$

Here $\boldsymbol{\epsilon} = [\epsilon_{\alpha\beta}]$ denotes the strain tensor field, $\mathbf{c} = [c_{\alpha\beta\mu\nu}]$ denotes the elastic constants tensor, and $\boldsymbol{\pi} = [\pi_{\mu\nu}]$ denotes the force dipole- or stress tensor field. The integrals comprise the bulk V or the surface S. The strain field $\boldsymbol{\epsilon}(\mathbf{r})$ is related to the displacement field $\mathbf{u}(\mathbf{r})$ by

$$\epsilon_{\alpha\beta}(\mathbf{r}) = \frac{1}{2} (\nabla_\alpha u_\beta(\mathbf{r}) + \nabla_\beta u_\alpha(\mathbf{r})). \quad (2.3)$$

Following [16] the stress field $\boldsymbol{\pi}(\mathbf{s})$ is superimposed of np different types $\boldsymbol{\pi}_{\mathbf{k}}(\mathbf{s})$

$$\boldsymbol{\pi}(\mathbf{s}) = \sum_{k=1}^{np} \boldsymbol{\pi}_{\mathbf{k}}(\mathbf{s}) = \sum_{k=1}^{np} \mathbf{P}_{\mathbf{k}} \rho_k(\mathbf{s}), \quad (2.4)$$

where we have introduced np different types of stress tensors $\mathbf{P}_{\mathbf{k}}$ and of adatom monomer or dimer densities $\rho_k(\mathbf{s})$.

On (100) surfaces with adatom positions of fourfold coordinated sites

$\mathbf{P}_1 = P_1[\delta_{\alpha\beta}]$ stand for an isotropic monomer stress tensor (or force dipole tensor),

$\mathbf{P}_2 = P_2[\delta_{\alpha 1} \delta_{\beta 1}]$ and $\mathbf{P}_3 = P_3[\delta_{\alpha 2} \delta_{\beta 2}]$ stand for anisotropic dimer stress tensors.

$\rho_1(\mathbf{s})$ then stands for the adatom monomer density distribution, $\rho_2(\mathbf{s})$ for the x-directed adatom dimer density distribution and $\rho_3(\mathbf{s})$ for the y-directed adatom dimer density distribution.

With Eq. (2.4) Eq. (2.2) reads

$$H_{\text{el}} = \frac{1}{2} \int_V \boldsymbol{\epsilon}(\mathbf{r}) \mathbf{c} \boldsymbol{\epsilon}(\mathbf{r}) d\mathbf{r} + \sum_{k=1}^{np} \int_S \boldsymbol{\epsilon}(\mathbf{s}) \mathbf{P}_{\mathbf{k}} \rho_k(\mathbf{s}) d\mathbf{s}. \quad (2.5)$$

The strain field $\boldsymbol{\epsilon}(\mathbf{r})$ is determined for given densities $\rho_k(\mathbf{s})$ by the requirement of mechanical equilibrium

$$\delta H_{\text{el}} / \delta u_\alpha(\mathbf{r}) = 0. \quad (2.6)$$

After an expansion in plane waves and calculations beyond the scope of this paper we end up at [16]

$$H_{\text{el}} = \frac{1}{2} \sum_{k=1}^{np} \sum_{l=1}^{np} \int_S \int_S \rho_k(\mathbf{s}) V_{kl}(\mathbf{s}, \mathbf{s}') \rho_l(\mathbf{s}') d\mathbf{s} d\mathbf{s}', \quad (2.7)$$

where the elastic interaction between adatoms (or dimers) of type k at \mathbf{s} and adatoms (or dimers) of type l at \mathbf{s}' $V_{kl}(\mathbf{s}, \mathbf{s}')$ will be given in Eq. (2.14).

2.3. Eigenvalue equation and elastic interaction

Recalling [16] the elastic interaction $V_{kl}(\mathbf{s}, \mathbf{s}')$ results from expanding the displacement field, given by freedom of stress in the bulk and freedom of stress normal to the surface, in plane waves. The vector

$$\mathbf{g}_m(\boldsymbol{\kappa}) = i\boldsymbol{\kappa} + \mathbf{n}q_m \quad (2.8)$$

denotes the sum of a wave vector $\boldsymbol{\kappa}$ parallel to the surface and a normal component. The normal vector \mathbf{n} should not be confused with the occupation numbers used in Eq. (2.1).

Freedom of stress in the bulk becomes

$$[c_{\alpha\beta\mu\nu}g_\beta^m g_\mu^m] a_\nu^m = 0, \quad (2.9)$$

where the \mathbf{a}_m are normalized eigenvectors. The label m denotes 3 displacement modes and the q_m are roots of the characteristic polynomial in q in Eq. (2.9). In this section m appears as lower index in vectors and as upper index in vector elements. Freedom of stress normal to the surface reads

$$[c_{\alpha\beta\mu\nu}n_\beta g_\mu^m a_\nu^m - \omega_{kl}^{-1}(\boldsymbol{\kappa})P_{\alpha\beta}^k P_{\mu\nu}^l g_\beta^m g_\mu^m a_\nu^m] A^{m,kl} = 0, \quad (2.10)$$

where the $\omega_{kl}(\boldsymbol{\kappa})$ are eigenvalues of the linear equations for all combinations of stress tensors $\mathbf{P}_k = [P_{\alpha\beta}^k]$. For further numerical treatment the eigenvalues are expanded in a cosine series

$$\omega_{kl}(\boldsymbol{\kappa}) = |\boldsymbol{\kappa}| \sum_{p=0}^{pmax} \omega_{kl,p} \cos(p\phi). \quad (2.11)$$

p attains the values 0, 4, 8 in the monomer case and 0, 2, 4 in the dimer case. ϕ is the angle between the x- and the $\boldsymbol{\kappa}$ direction. The $\omega_{kl,p}$ are proportional to the product of stress parameters $P_k P_l$ and inverse proportional to the elastic constant c_{44}

$$\omega_{kl,p} \sim P_k P_l / c_{44}. \quad (2.12)$$

The elastic interaction $V_{kl}(\mathbf{s}, \mathbf{s}')$ in Eq. (2.10) is given by [16]

$$V_{kl}(\mathbf{s}, \mathbf{s}') = (2\pi)^{-1} \sum_{p=0}^{pmax} \omega_{kl,p} \cos(p\chi) \cos(p\pi/2) \int_0^{\kappa_B} \kappa^2 J_p(\kappa s) d\kappa, \quad (2.13)$$

where J_p are Bessel functions of the order p , $s = \text{Abs}(\mathbf{s} - \mathbf{s}')$ in units of the lattice constant s_0 , and χ is the angle between the x- and the $\mathbf{s} - \mathbf{s}'$ direction.

The κ integral over the Bessel function $J_p(\kappa s)$ in Eq. (2.13) extends over the Brillouin zone and requires special attention. The Brillouin zone is assumed circular to allow for a closed solution. In the earlier approach [12] a smooth cutoff lead to an interaction attractive in the short range and repulsive with a s^{-3} law. Such interaction does not fit to the DFT results in [8]. A step cutoff produces an oscillating interaction with a $s^{-3/2}$ law and convergence problems when performing lattice sums. The way out is an intermediate cutoff and an oscillating interaction with a s^{-3} law, approximated by

$$V_{kl}(s, \chi) = (2\pi)^{-1} \sum_p \omega_{kl,p} \cos(p\chi) \cos(p\pi/2) 2^{-1-p} \kappa_B^3 (s\kappa_B)^p \Gamma\left(\frac{3+p}{2}\right) * \\ {}_pF_q\left(\left(\frac{3+p}{2}\right), \left(\frac{5+p}{2}, 1+p\right), -\frac{1}{4}s^2\kappa_B^2\right) / \left(1+s^{3/2}\right), \quad (2.14)$$

where $\Gamma(p)$ denotes the Gamma function and ${}_pF_q(a,b,z)$ the generalized hypergeometric function.

2.4. Eigenvalues for Pd(100)

Tab.1 shows the coefficients $\omega_{kl,p}$ for Pd(100) using elastic constants $c_{11}=221$, $c_{12}=171$, $c_{44}=70.8$ GPa [20]. We note the units of the $\omega_{kl,p}$:

- the numerator is $P_k P_l$, the product of the scalar parameters P_k and P_l (force dipole constants) introduced in section 2.1, describing the lateral stress magnitude an adatom monomer or a dimer exerts to the surface
- the denominator is the c_{44} elastic constant of the substrate.

k	l	$\omega_{kl,0}$	$\omega_{kl,2}$	$\omega_{kl,4}$	$\omega_{kl,8}$
1	1	-0.9431		0.1009	0.0016
1	2	-0.66577	-0.73706	-0.07129	
2	2	-1.1521	-1.0424	0.1097	
1	3	-0.66577	0.73706	-0.07129	
2	3	0.21057	0.	-0.21057	
3	3	-1.1521	1.0424	0.1097	

Table 1. Coefficients $\omega_{kl,p}$ (in $P_k P_l / c_{44}$ units) on Pd(100)

The $k=l=1$ coefficients belong to a monomer-monomer (pair) interaction. The $k=1$, $l=2,3$ coefficients belong to monomer-dimer (trio) interactions, we note the opposite sign of the $p=2$ values and the identical $p=0$ and $p=4$ values.

The $k=2,3$, $l=2,3$ coefficients belong to dimer-dimer (quattro) interactions, we note the opposite sign of the $p=2$ values and the identical $p=0$ and $p=4$ values for $k=l=2$ and $k=l=3$ respectively.

The above values reflect symmetries on the (100) surface.

3. Lattice sum

In the following the elastic energy will be formulated as lattice sums for 3 parts, consisting of

- a monomer-monomer part
- a dimer-dimer part
- a monomer-dimer part

which allows to independently inspect the influence of the stress parameters P_1 and P_2 on the elastic energy and to perform their fit to DFT configuration energies finally.

3.1. Elastic energy of adatom configurations

A configuration of m adatom monomers on a discrete lattice of substrate positions $\{\mathbf{s}_i\}$ is described by the monomer density

$$\rho_1(\mathbf{s}) = \sum_{i=1}^m \delta(\mathbf{s} - \mathbf{s}_i) n_i \quad (3.1)$$

with $n_i \in \{0, 1\}$ denoting occupation numbers of lattice positions \mathbf{s}_i and $\delta(\mathbf{s} - \mathbf{s}_i)$ is the Dirac Delta function. The n_i should not be confused with the normal vector in section 2.

While the monomer stress tensor \mathbf{P}_1 is located at the adatom lattice points, the dimer stress tensors \mathbf{P}_2 and \mathbf{P}_3 are located between two nearest neighbor adatoms. The density of an x-directed adatom dimer configuration of type $k=2$ with occupation numbers n_i and n_{ix} and positions at the center of nearest neighbor positions $\{\mathbf{s}_i\}$ and $\{\mathbf{s}_{ix}\}$ is given by

$$\rho_2(\mathbf{s}) = \sum_{i=1}^m \delta(\mathbf{s} - \mathbf{s}_i - \Delta_x) n_i n_{ix}. \quad (3.2)$$

Here we have defined $\Delta_x = (\mathbf{s}_{ix} - \mathbf{s}_i)/2$. Likewise the density of an y-directed adatom dimer configuration of type $k=3$ with positions at the center of nearest neighbor positions $\{\mathbf{s}_i\}$ and $\{\mathbf{s}_{iy}\}$ is given by

$$\rho_3(\mathbf{s}) = \sum_{i=1}^m \delta(\mathbf{s} - \mathbf{s}_i - \Delta_y) n_i n_{iy}. \quad (3.3)$$

Here we have defined $\Delta_y = (\mathbf{s}_{iy} - \mathbf{s}_i)/2$. With Eqs. (3.2), (3.3) and (2.7) the elastic energy of the m adatom configuration reads

$$H_{el} = H_{11} + H_{12} + H_{13} + H_{22} + H_{23} + H_{33}, \quad (3.4)$$

with

$$H_{11} = \sum_{i=1}^m \sum_{j=2}^i V_{11}(\mathbf{s}_i, \mathbf{s}_j) n_i n_j \quad (3.4.a)$$

$$H_{12} = \sum_{i=1}^m \sum_{j=1}^m V_{12}(\mathbf{s}_i, \mathbf{s}_j + \Delta_x) n_i n_j n_{jx} \quad (3.4.b)$$

$$H_{13} = \sum_{i=1}^m \sum_{j=1}^m V_{13}(\mathbf{s}_i, \mathbf{s}_j + \Delta_y) n_i n_j n_{jy} \quad (3.4.c)$$

$$H_{22} = \sum_{i=1}^m \sum_{j=1}^i V_{22}(\mathbf{s}_i + \Delta_x, \mathbf{s}_j + \Delta_x) n_i n_{ix} n_j n_{jx} \quad (3.4.d)$$

$$H_{23} = \sum_{i=1}^m \sum_{j=1}^m V_{23}(\mathbf{s}_i + \Delta_x, \mathbf{s}_j + \Delta_y) n_i n_{ix} n_j n_{jx} \quad (3.4.e)$$

$$H_{33} = \sum_{i=1}^m \sum_{j=1}^i V_{33}(\mathbf{s}_i + \Delta_y, \mathbf{s}_j + \Delta_y) n_i n_{iy} n_j n_{jy} \quad (3.4.f)$$

Comparing (3.4) with the Hamiltonian used in [8] we note

- the elastic expansion (3.4) comprises pair- V_{11} , trio- V_{1x} , quattro- V_{xy} interactions but no higher ones
- the $V_{kl}(\mathbf{s}_i, \mathbf{s}_j)$ are the equivalents to the lateral interactions in [8].

Eq. (2.12) allows to regroup Eq. (3.4) as sum of elements depending on the parameters P_1 and P_2 for fitting purposes

$$H_{\text{el}} = P_1 P_1 h_{11} + P_1 P_2 h_{12} + P_2 P_2 h_{22}. \quad (3.5)$$

The coverage dependent binding energy per adatom E_b is the sum of the binding energy of an isolated adatom $E_b^{\text{on-site}}$ and of its interaction energy, in the present model

$$E_b = E_b^{\text{on-site}} + H_{\text{el}}/m. \quad (3.6)$$

$E_b^{\text{on-site}}$ in the present model contains the self term $V_{11}(\mathbf{s}_i, \mathbf{s}_i)$, describing the strain energy of an isolated adatom.

3.2. Adatom configurations on Pd(100)

The lattice sums in Eq. (3.4) have been evaluated for the 5 hollow site binding energies as published in [8]. For the elastic model the stress parameters P_1 and P_2 together with the Brillouin zone limit κ_B have been fitted to the known binding energies. The sums have been truncated for elements with $|\mathbf{s}_i - \mathbf{s}_j| > 25s_0$.

The DFT calculated binding energies of [8] and the fitted binding energies for $P_1=9.225$, $P_2=4.151$, both in $c_{44}s_0^3$ units, and for $\kappa_B=6.047s_0^{-1}$, are compared in Tab. 2. The elastic model seems to reasonably interpret the few binding

energies available. $E_b^{\text{on-site}}$ could not be calculated directly in DFT; its value in [8] was chosen identical to the DFT binding energy at 1/9 coverage, assuming zero interaction for configurations with smaller coverage. The elastic model, of course, shows a lower on-site energy.

bindingenergy/meV	coverage/ML	DFT	elasticmodel
$E_b^{\text{on-site}}$	0	-1249	-1265
$(3\times 3) - O$	1/9	-1249	-1228
$p(2\times 2) - O$	1/4	-1348	-1359
$c(2\times 2) - O$	1/2	-1069	-1079
$(2\times 2) - 3O$	3/4	-643	-643
$(1\times 1) - O$	1	-344	-344

Table 2. Binding energies per adatom in meV units for O-Pd(100) configurations calculated by DFT [8] and using the present elastic model.

The elastic model with the above parameter set will now be used to derive further features of the O-Pd(100) system up to half coverage. In Tab.3 the pair interactions from [8] are compared with those of the present elastic Hamiltonian up to the 9th nearest neighbors. The optimum set of [8] truncates interactions beyond the 5th nearest neighbors while in the elastic model the interactions range to infinity - with decreasing magnitude. The values of the three nearest neighbor interactions are in consequence about half but equal in sign. We also note the variances in the value sets of [8] due to their ill-conditioned configuration matrices. The oscillation wavelenght for the $p=0$ term in Eq. (2.14) with κ_B as found in the fit is close to the lattice constant s_0 .

pairinteraction/meV	optimumset	elasticmodel
$n.n.$	292	135
$2n.n.$	90	45
$3n.n.$	-50	-27
$4n.n.$	-10	-12
$5n.n.$	0	13
$6n.n.$	0	6
$7n.n.$	0	-2
$8n.n.$	0	-6
$9n.n.$	0	5

Table 3. Pair interactions in meV units for O-Pd(100) nearest neighbors, taken from the optimum set in [8] and using the present elastic model.

The $p=0$ pair interaction term in Eq. (2.14) with the above parameter set is

- repulsive in the 0.6 to 1.1 s_0 and the 1.7 to 2.2 s_0 regions
- attractive in the $<0.6 s_0$, 1.2 to 1.6 s_0 and 2.2 to $2.6s_0$ regions.

Trio- and quattro interactions appear relevant close to half coverage when adatom dimers show up. They are relevant for interpreting the high coverage binding energies and for the calculation of 3- and 4 adatom clusters containing dimers. Table 4 shows the elastic interaction energy per adatom for some of those clusters. The trio terms stem from the short range interaction created by the strain of isolated adatoms with the strain of pairs. The quattro term of the

first 3-adatom cluster stems from the strain created by the pairs in line; in the case of rectangular pairs the quattro term is negligible. The quattro terms of 4-adatom clusters differ in sign because in the first case the pairs are parallel (with attractive interactions) while in the second case 3 adatoms stand in line (with repulsive interaction). Such cluster energies provide a test case for DFT calculations. The elastic energies of clusters appear to be about half the values shown in [8].

configuration	pair	trio	quattro	sum
$(-1, 0)(0, 0)(1, 0)$	81	10	29	120
$(1, 0)(0, 0)(0, 1)$	105	2	0	107
$(-1, 1)(0, 0)(1, 0)$	56	-4	0	52
$(0, 1)(0, 0)(2, 0)$	33	-1	0	32
$(0, 1)(0, 0)(1, 0)(1, 1)$	158	6	-10	154
$(-1, 0)(0, 0)(1, 0)(0, 1)$	117	10	22	149

Table 4. Elastic interaction energy per adatom in meV units for oxygen clusters on Pd(100). Configurations are indicated by primitive cell coordinates; pair-, trio- and quattro contributions are shown with their sum.

Values for trio- and quattro interactions are ignored in the subsequent near order analysis while not relevant in the coverage region well below 0.5 monolayer.

4. Near order analysis

While the frequently used Monte Carlo method determines thermodynamic functions by averaging over many simulation passes, a direct statistical method will be used in this section to analyze the near order of adatoms for varying coverages and temperatures. The above elastic interaction will form the basis.

4.1. Adatom pair distribution calculation method

In this section we make use of the closed solution (2.14) for the adatom-adatom interaction $V_{kl}(\mathbf{s}, \mathbf{s}')$ with adatom positions on a lattice. The strong nearest neighbor repulsion makes the creation of nearest neighbor adatom dimers unlikely up to half coverage and allows to restrict attention to the pair interaction $V_{11}(\mathbf{s}, \mathbf{s}')$ in the region below. For clarity we adapt the notation and denote $U_{ik}=U_{ik}(\mathbf{s}_i, \mathbf{s}_k)=V_{11}(\mathbf{s}_i, \mathbf{s}_k)$, the pair interaction between adatoms i at location \mathbf{s}_i and k at location \mathbf{s}_k .

The probability for finding an adatom at a certain lattice site equals the coverage θ if the adatoms are uncorrelated. If adatoms are correlated e.g. due to an interaction, the probability pr to find an adatom at position \mathbf{s}_2 if another is located at position \mathbf{s}_1 is

$$pr(\mathbf{s}_1, \mathbf{s}_2) = \theta g(\mathbf{s}_1, \mathbf{s}_2). \quad (4.1)$$

The pair distribution $g(\mathbf{s}_1, \mathbf{s}_2) = g_{12}$ for atoms interacting in a volume

in Kirkwoods superposition approximation is given by the Born-Green-Yvon integro-differential equation [17]

$$\nabla^{(1)} [\ln g_{12} + u_{12}] = -\rho \int_V g_{23} g_{13} \nabla^{(1)} u_{13} d\mathbf{r}_3 \quad (4.2)$$

Here $u_{12}=U_{12}/k_B T$ denotes the scaled pair interaction, ρ is the density, and $\nabla^{(1)}$ acts on the coordinates of atom (1) only. The left hand side of (4.2) describes the familiar zero coverage Boltzmann distribution while the right hand side of (4.2) introduces the nonlinear density dependent correlation. Following [18] this equation in the actual 2-d case can be transformed into an integral equation

$$\ln g_{12} + u_{12} = \frac{1}{2\pi} \theta \int_S (g_{23} - 1) d\mathbf{s}_3 \int_S g_{43} \frac{\mathbf{s}_{14} \nabla^{(4)}}{\mathbf{s}_{14} \mathbf{s}_{14}} u_{43} d\mathbf{s}_4 \quad (4.3)$$

with θ denoting the adatom coverage. This non linear equation for g_{12} turns out to be unstable for coverages θ above 0.1 to 0.2 ML for the studied interaction and temperature range. To extend the reach of the pair distribution analysis towards nearly half coverage we introduce a heuristic θ^2 term utilizing the adatom-vacancy symmetry for adatom pair interactions at half coverage

$$\bar{g}_{12}(0.5) = g_{12}(0.5) \quad (4.4)$$

with \bar{g} denoting the vacancy distribution function, in the pair interaction case following

$$\ln \bar{g}_{12} + \bar{u}_{12} = \frac{1}{2\pi} \bar{\theta} \int_S (\bar{g}_{23} - 1) d\mathbf{s}_3 \int_S \bar{g}_{43} \frac{\mathbf{s}_{14} \nabla^{(4)}}{\mathbf{s}_{14} \mathbf{s}_{14}} \bar{u}_{43} d\mathbf{s}_4, \quad (4.5)$$

where

$$\bar{\theta} = 1 - \theta, \quad \bar{u}_{12} = -u_{12}, \quad \nabla^{(1)} \bar{u}_{43} = -\nabla^{(1)} u_{43}. \quad (4.6)$$

Eq. (4.4) is fulfilled by Eq. (4.3) modified by an additional θ^2 term

$$\ln g_{12} = -u_{12} + \theta I_{12} + \theta^2 (4u_{12} - 2I_{12}), \quad (4.7)$$

where

$$I_{12} = \frac{1}{2\pi} \int_S (g_{23} - 1) d\mathbf{s}_3 \int_S g_{43} \frac{\mathbf{s}_{14} \nabla^{(4)}}{\mathbf{s}_{14} \mathbf{s}_{14}} u_{43} d\mathbf{s}_4. \quad (4.8)$$

In the case of half coverage Eq. (4.7) predicts $g_{12}=1$, a consequence of omitting trio- and quattro interactions in this analysis. Conclusions in the range near $\theta=0.5$ should be taken with this restriction in mind. The non linear integral equation (4.7) for g_{12} could be solved numerically for elevated temperatures. Starting from $\theta=0$ the coverage was incremented by small steps of 0.005 until half coverage was reached. Each calculated pair distribution was input for the subsequent step. The results are presented in the following section.

To enable a comparison with LEED measurements of the O-Pd(100) system the Fourier Transform $\tilde{\nu}$ of the correlation $\nu_{12}=g_{12}-1$ was calculated as well. The correlation $\nu_{12}(s)$ between two adatoms is expected to decrease rapidly as their distance s increases, while $g_{12}(s)$ approaches 1 for large distances.

4.2. Temperature scaling

Eqs. (4.7) and (4.8) allow to deduce the pair distribution at temperature T_1 , $g_{12}(T_1)$, from that calculated for the temperature T_0 . With

$$u_{12}(T_1) = u_{12}(T_0) - T_0/T_1 \quad (4.9)$$

Eq. (4.7) can be written

$$\ln g_{12}(T_1) = (-u_{12}(T_0) + \theta I_{12}(T_0) + \theta^2 (4u_{12}(T_0) - 2I_{12}(T_0))) T_0/T_1. \quad (4.10)$$

So

$$g_{12}(T_1) = g_{12}(T_0)^{(T_0/T_1)}. \quad (4.11)$$

If temperatures are reduced, pair distribution values above 1 grow, while values below 1 decrease. This allows to extrapolate pair distributions to low temperatures at which Eqs. (4.7) and (4.8) do not converge. Such extrapolation, however, has to consider Eq. (4.1) and the probability restriction $pr < 1$ for all values of g_{12} .

4.3. Adatom pair distribution results

The pair distribution according to Eq. (4.1) is a measure for the probability to find an adatom at position \mathbf{s}_2 if another is located at position \mathbf{s}_1 . Evaluating Eqs. (4.7, 4.8) with the pair interaction of Eq. (2.14) results in a g_{ik} matrix for lattice positions (i, k) of adatom 2, if adatom 1 is located at $(0, 0)$. While further distant adatoms approach $g_{ik}=1$, the near neighbors values differ from 1. The $g_{ik}(\theta=0)$ values correspond to pair interaction values V_{ik} of Tab.3.

Fig. 1.a shows for the temperature 400K $g_{ik}(\theta)$ for the nearest to the 5th nearest neighbors. The nearest neighbor values according to strong repulsion are small up to 0.4 ML. The 2nd nearest neighbor values according to repulsion are slowly increasing towards 1. The 3rd nearest neighbor values represent attracting adatoms and decrease from 2.18 at zero coverage to 1.37 at 0.25 ML, slowly approach 1.24 at 0.4 ML and reaches 1 at 0.5 ML. The maximum probability $pr \approx 0.52$ of finding an adatom at a 3rd nearest neighbor position is at 0.4 ML coverage. The 4th nearest neighbor values decrease towards 1.04 at 0.25 ML and remain nearly flat until 0.5 ML. They represent weakly attracting adatoms. The 4nn g_{ik} values slightly above 1 don't indicate a p(2x2) structure. The 5th nearest neighbor values are almost flat till 0.25 ML and rise to 1 at 0.5 ML. Without showing in the picture we note pair distribution values rising to 1.25 at 0.1 ML for the attracting 8th neighbor interaction (cf. Tab. 3).

Fig. 1.b shows for the temperature 400K the maximum of the corresponding Fourier transformed correlation $\tilde{\nu}$ at $(0, 1/2)$, the p(2x2) LEED spot. It decreases slowly till 0.35 ML coverage and falls towards zero at half coverage. It shows qualitative agreement with LEED measurements [19]. Overall the correlation $\tilde{\nu}$ shows a square like structure with small broad hills. At $(1/2, 1/2)$, respective p(2x2)+c(2x2), no spot is visible. Again we note the pair interaction restrictions.

The $g_{ik}(\theta)$ calculations do not show a long range order of adatoms at 400K. The LEED measurements at similar temperatures in [19] have been interpreted by longer range ordered phases. Not knowing the details of the measurements the differences could stem from ignoring tri- and quattro interactions.

The temperature dependency of the pair distribution g_{ik} is given by Eq. (4.11). If temperature is lowered, the g_{ik} values for 3rd and 4th nearest neighbors increase. If temperature is increased, the extrapolation is limited when Oxygen desorption starts at 700K at low coverage and is almost completed at 900K [19]; in this region the g_{ik} values are approaching 1, the disordered state.

The corresponding temperature dependency of the Fourier transformed correlation $\tilde{\nu}$ is not a simple power law. With increasing temperature it shows an even stronger decrease towards zero.

From Fig. 1.a we conclude a high amount of $((0,0),(2,0))$ 3rd neighbor pairs and a considerable amount of $((0,0),(2,1))$ 4th neighbor pairs in equilibrium at lower coverage at 400 K. Isolated adatoms and other pair configurations appear less frequently.

4.4. Adatom 3-body distribution

The Kirkwood approximation

$$g(\mathbf{s}_1, \mathbf{s}_2, \mathbf{s}_3) = g(\mathbf{s}_1, \mathbf{s}_2) g(\mathbf{s}_2, \mathbf{s}_3) g(\mathbf{s}_3, \mathbf{s}_1) \quad (4.12)$$

utilized in Eq. (4.3) allows to derive 3-adatom distributions providing additional insight on equilibrium cluster formation especially in the lower coverage region. Fig. 2 shows the 5 top value 3-body distributions g_{ijk} for the temperature 400 K as a function of coverage. In short Fig. 2 shows: straight triplets are preferred over triplets with angles; the rectangular triplet - the base of a p(2x2)-O lattice - is the least probable of the sample at coverages greater than 0.05 ML.

5. Discussion

In this section limitations and applicability and of the model are reviewed, the results of numerical calculations are discussed and aspects for further research are sketched.

5.1. Restrictions and limitations of the model

The model is based on the theory of elasticity in the substrate and on the lateral stress adatoms apply to the surface. Key assumption is the mechanism by which adatoms and dimers interact. Monomer adatoms sitting on fourfold adatom sites expand or contract the substrate by creating isotropic stress. Trio- and quattro interactions are due to the anisotropic stress adatom pairs exert to the substrate when they are bound electronically and stretched (or compressed) due to their position on substrate sites.

The unknown electronic binding energy of adatom pairs is ignored in the present model. Adatom dipole-dipole interactions may also play a role.

An elastic continuum model for the substrate may be rated inadequate for describing short range effects, but describes well long range effects and elastic anisotropies (strong in case of adatom dimers). The cutoff mechanism used in Eq. (2.14) avoids a s^{-3} singularity and therefore extends the models reach towards small distances. Assuming a circular Brillouin zone is a risk, so Eq. (2.14) can only be an approximation. The search for a most realistic cutoff function is currently left open.

The restriction to high symmetry adatom locations has the advantage of stress parameter P_k degeneracy. On (100) surfaces $P_3=P_2$ due to the equivalence of x-directed and y-directed dimers. This reduces the number of free model parameters. The dependence of stress parameter values P_k from coverage could be an issue. Its value for isolated dimers could differ from its value in islands since the bond between adatoms depends on their coordination.

A further key assumption is an ideal flat surface, i.e. the absence of steps which are known for their significant attractive or repulsive interaction with adatoms.

The present model parameters rely on the DFT calculations in [8]. The adatom configuration base and their DFT energies used in this paper are restricted to the 5 configurations published and thus are not at all exhaustive, but allow a first glance on their elastic energy. Utilization of the full range of the DFT energy results in [8] would allow a consistency proof. The methods used to derive adatom interactions and their near order should remain valid also in case of a broader base.

The existence of long range elastic interactions would imply significant influence of the super-cell size used in the DFT calculations used in [8]. Variations of the slab size could prove size effects to the configuration energies.

Utilization of the 2-dimensional version of the BGY equation [18] for calculating the adatom pair distribution provides insights complementary to the Monte Carlo simulations in [8]. Its usage in a lattice grid seems to be valid beyond a certain temperature. Its adaptation for the region between 0.1 and half coverage avoids numeric stability problems but still needs a better foundation and consideration of trio- and quattro interactions in the region between 0.4 and 0.5 ML coverage. Due to surface reconstruction above half coverage the current approach, however, seems reasonable especially below 0.4 ML coverage. The striking convergence of the pair distribution towards 1 at half coverage is

a consequence of the adatom-vacancy symmetry assumed, ignoring trio- and quattro interactions.

5.2. Calculation results

The model of strain mediated interacting oxygen adatoms turns out to interpret well the binding energies of O on Pd(100) calculated with DFT methods. The few free model parameter support the validity of the elastic model. In consequence the concept of a lattice-gas Hamiltonian without considering the possibility of long range interactions appears questionable.

Tab. 3 shows only a few nearest neighbor elastic model pair interactions, many more neighbors have been used when calculating the binding energies shown in Tab. 2.

The results for the interaction of dimers with monomers or dimers in Tab. 4 show about half the values for interactions in [8]. Such reduced values could avoid the $T_c(\theta)$ anomaly obtained with large interaction values in [8]. We note that in [8] only those adatom clusters show significant trio- and quattro interaction values which contain nearest neighbor dimers.

Fig. 1.a indicates at 400 K the slope of near neighbor pair distributions towards disorder at half coverage. The models disorder prediction at half coverage is a consequence of ignoring trio- and quattro interactions.

The three-body distributions at 400 K in Fig. 2 indicate the probability of different cluster configurations. The lack of a predominant cluster configuration indicates that clusters form glassy islands coalescing near 0.25 ML coverage. Thermal movement would make their form and structure dynamic. Beyond 0.25 ML second neighbor vacancies would be filled statistically. Local $((1,1),(1,-1))$ grids are not visible in the present approximation. Overall the existence of different phases and consequently a critical temperature is put in question for the O-Pd(100) system.

The scaling features of Eq. (4.11) allows extrapolation of the pair distribution to lower and higher temperatures. At elevated temperatures the local order has nearly been melting.

The lack of long range order predicted by the current elastic model corresponds with an Ising model including long range interactions [21].

Overall the calculations lack detailed experimental verification. This shortcoming deserves cooperation with experimental groups.

5.3. Open questions and further aspects

The limits of the continuous theories used, both for elasticity and for the pair distribution, need a more solid foundation.

The search for a cutoff function between a smooth exponential and a hard Heaviside function could lead to an oscillating interaction with a proper decay.

DFT calculations of 2, 3, 4 adatom clusters could provide insights complementary to calculations of ordered adatom structures. They could directly be compared with the elastic energies of Tab. 4 and act as proof.

A theoretical (DFT) model to determine the magnitude of the stress parameters P_k could determine the elastic adatom interaction directly.

The DFT calculations [8] using a finite slab should be varied in size to cover long reach effects.

The numeric stability when evaluating Eq. (4.7) is a problem for temperatures below 300K when simultaneously the population probability $g_{ik}\theta$ approaches 1. Smaller step sizes and an extended range when evaluating Eq. (4.7) do not improve stability significantly. It seems that only an improved methodology for handling the discrete lattice nature would really help.

The rising pair distribution values for nearest neighbors indicate that trio- and quattro interactions play a role close to half coverage. The near range order analysis would need trio- and quattro term extensions for such analysis.

Other substrate materials than Pd with different elastic constants and different types of adatoms may be interesting to compare the theory with a broader range of experimental findings.

The interaction of monomers and dimers consisting of different adatom species is in principle covered by the elastic theory, simulations could help to assess its applicability.

Availability of more LEED data would enable a better comparison between measurements and theory.

A more solid foundation of the model would form the basis to derive more thermodynamic properties of O-Pd(100).

The influence of dynamic glassy surface structures on their catalytic activity seems to be an interesting topic. When discussing adatom diffusion, the influence of substrate strain on their activation energy should be considered.

6. Summary

The binding energies of five different O-Pd(100) configurations, calculated by first principles methods [8], have been successfully interpreted by a Hamiltonian of substrate strain mediated interactions comprising pair-, trio-, and quattro terms with a few free parameters. It is concluded that the often used method of building a Hamiltonian without considering longer range interactions is dangerous and can be misleading. The adatom near order was evaluated by calculating the pair distribution or population probability using an adapted statistical method. Pair distributions of few nearest neighbors are shown dependent on coverage and temperature. Together with three-body distributions they provide a glance on the adatom near order. Comparison with LEED measurements shows qualitative agreement but differences in their interpretation. Limitations of the model are analyzed and open questions are addressed.

References

- [1] T.L.Einstein, Interactions between Adsorbate Particles, in: Physical Structure of Solid Surfaces (W.N.Unertl ed.), Elsevier, Amsterdam (1996)
- [2] J.V.Barth, G.Costantini, K.Kern, Nature 437, 671 (2005)
- [3] H.Brune, Creating Metal Nanostructures at Metal Surfaces Using Growth Kinetics, in: Handbook of Surface Science Vol.3 (E.Hasselbrink and B.I.Lundqvist ed.), Elsevier, Amsterdam (2008)
- [4] H.Ibach, Surf.Sci.Rep. 29, 195 (1997)
- [5] F.Komori, S.Ohno, K.Nakatsuji, Progr. Surf. Sci. 77, 1 (2004)
- [6] R.I.Masel, Principles of Adsorption and Reaction on Solid Surfaces, Wiley, New York (1996)
- [7] K.Reuter, C.Stampfl, M.Scheffler, Ab Initio Atomistic Thermodynamics and Statistical Mechanics of Surface Properties and Functions. In: Handbook of Materials Modelling, Part A. Methods, (Ed.) S.Yip, Springer, Berlin (2005)
- [8] Y.Zhang, V.Blum, K.Reuter, Phys. Rev. B 75, 235406 (2007)
- [9] M.Todorova, E.Lundgren, V.Blum, A.Mikkelsen, S.Gray, J.Gustafson, M.Borg, J.Rogal, K.Reuter, J.N.Andersen, M.Scheffler, Surf. Sci. 541, 101 (2003)
- [10] W.-X.Li, C.Stampfl, M.Scheffler, Phys.Rev.B 65, 075407 (2002)
- [11] K.H.Lau, W. Kohn, 1977, Surface Sci. 65, 607 (1977)
- [12] W.Kappus, Z.Physik B 29, 239 (1978)
- [13] K.H.Lau, Sol. State Commun. 28, 757 (1978)
- [14] H.Horner, H.Wagner, Adv. in Phys. 23,587 (1974)
- [15] P.Müller, A.Saul, Surf. Sci. Rep. 54, 157 (2004)
- [16] W.Kappus, arXiv 1610.07326
- [17] M.Born, H.S.Green, Proc. Roy. Soc. (London) A188, 10 (1946)
- [18] W.Kappus, J.Phys.C: Solid State Phys. 11, L565 (1978)
- [19] S.-L.Chang, P.A.Thiel, J. Chem. Phys. 88, 2071 (1988)
- [20] A.G.Every, A.K.McCurdy: Table 3. Cubic system. Elements. D.F.Nelson(ed.), SpringerMaterials-The Landolt-Börnstein Database (2012)
- [21] T.Nakada, P.A.Rikvold, T.Mori, M.Nishino S.Miyashita, Phys.Rev.B 84, 054433 (2011)

Acknowledgement

This work is dedicated to my grandchildren. Continuous support of my family is gratefully acknowledged.

Figures

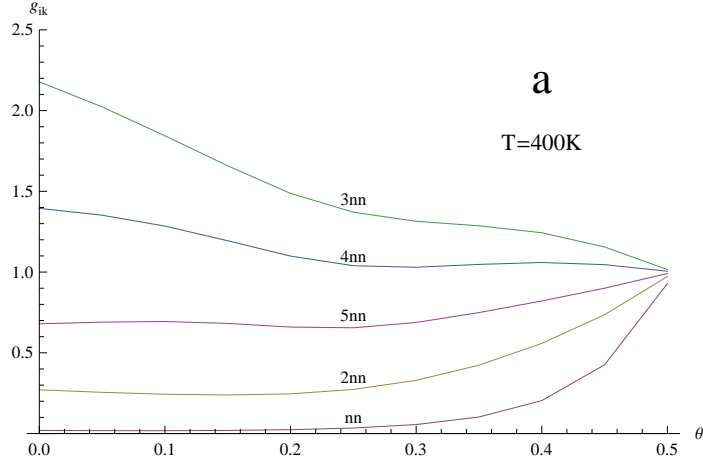


Fig. 1.a: Adatom pair distribution $g_{ik}(\theta)$ at 400K from nearest to 5th nearest neighbors in dependence of coverage θ .

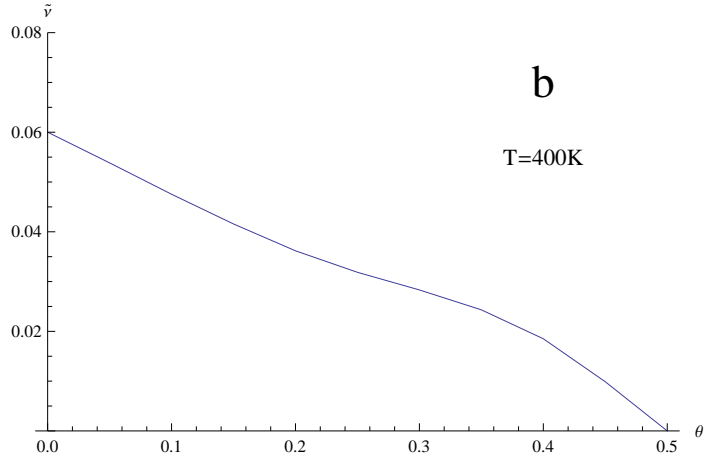


Fig. 1.b: Fourier transformed correlation $\tilde{\nu}$ at $(0, 1/2)$, the p(2x2) LEED spot, at 400K in dependence of coverage θ .

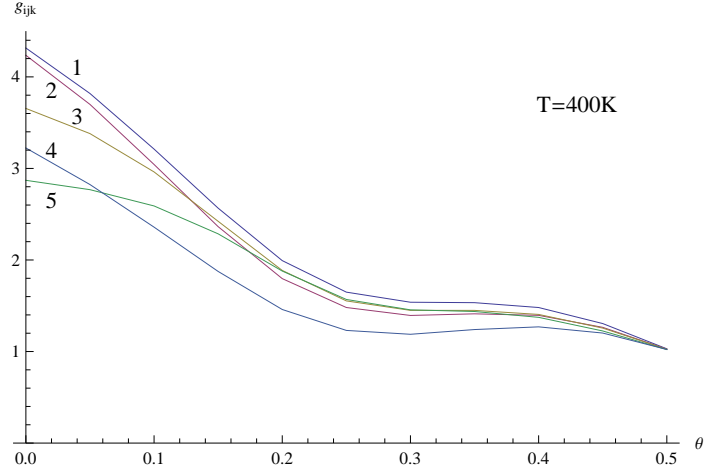


Fig. 2: Three-body distribution g_{ijk} for the 5 top value configurations at 400K in dependence of coverage θ .

The numbers 1 to 5 indicate top value trimers, identified by primitive cell coordinates:

1: $((2,0),(0,0),(-2,0))$; 2: $((2,0),(0,0),(1,2))$; 3: $((2,0),(0,0),(-1,2))$; 4: $((2,0),(0,0),(0,2))$; 5: $((2,0),(0,0),(-2,3))$.

© Wolfgang Kappus (2016)